Radial Motion Control of Axial-Flux Self-Bearing Motor Using Plus and Minus Two-Pole Magnetic Fields

Satoshi Ueno[1], Yuki Yamamoto[2], and Changan Jiang[3]

[1] RItsumeika University, Kusatsu, Shiga, Japan
sueno@se.ritsumei.ac.jp
[2] Ritsumeikan University, Kusatsu, Shiga, Japan
[3] Osaka Institute of Technology, Osaka, Japan
changan.jiang@oit.ac.jp

Abstract

This paper introduces an axial-flux self-bearing permanent magnet motor that controls motor torque, axial force, radial forces, and tilting moments by a single stator. A rotating magnetic field with the same pole number as the rotor controls the motor torque and axial force. Rotating magnetic fields with the rotor' s pole number plus and minus two poles control the radial forces and tilting moments. These fields generate both radial forces and tilting moments, and the direction of one of them becomes the same, and the other becomes opposite. Hence, we can control the radial forces and tilting moments independently. This paper describes the theoretical analysis of the radial forces and tilting moments and derives the control currents of stator windings. Levitation and rotation tests of a prototype motor confirm the proposed method.

1 Introduction

An axial-flux self-bearing motor (AFSBM) is a combination of a disk type permanent magnet (PM) motor and active magnetic bearings and can simultaneously control both the motor torque and position of the rotor [5]. One-, three-, and five-degrees-of-freedom (DOF) active-controlled AFSBMs have been proposed.

The one-DOF active-controlled AFSBM controls motor torque and axial force by q- and d-components of a magnetic field with the same pole number of the rotor. The three-DOF active-controlled AFSBM utilizes the magnetic field with plus or minus two poles to control the tilting moments of the rotor [2]. However, these fields generate not only the tilting moment but also the radial force to the rotor. Therefore, it is necessary to use a sandwich structure to cancel the radial force or adjust the center of gravity (COG) of the rotor to ensure the stability of tilt control [3].

On the other hand, by utilizing this characteristic five-DOF active-control can be realized. Osa et al. have developed the five-DOF active-controlled AFSBM for small size artificial heart pump [1]. However, this motor requires a sandwich structure to control both the radial forces and tilting moments and restricts the design of the whole device. To solve this problem, we have proposed the different type five-DOF active-controlled AFSBM that uses unipolar and four-pole magnetic fields to control the radial force and tilting moment for a two-pole PM rotor [4]. Since the proposed motor does not require a sandwich structure, it can improve the flexibility of design. However, this AFSBM requires two pairs of the rotor and stator, then the mechanism and controller became complex.

This paper introduces a novel AFSBM that uses plus and minus two-pole magnetic fields to control the radial forces and tilting moments to realize a simple structure. Since the proposed method requires only a pair of the rotor and the stator, the structure becomes simple.

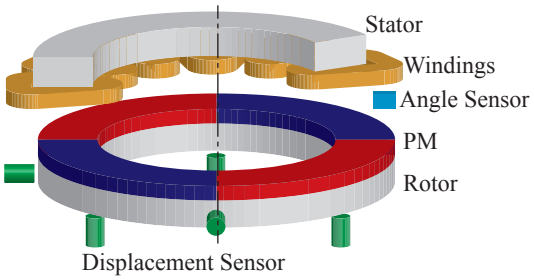

Figure 1: Structure.

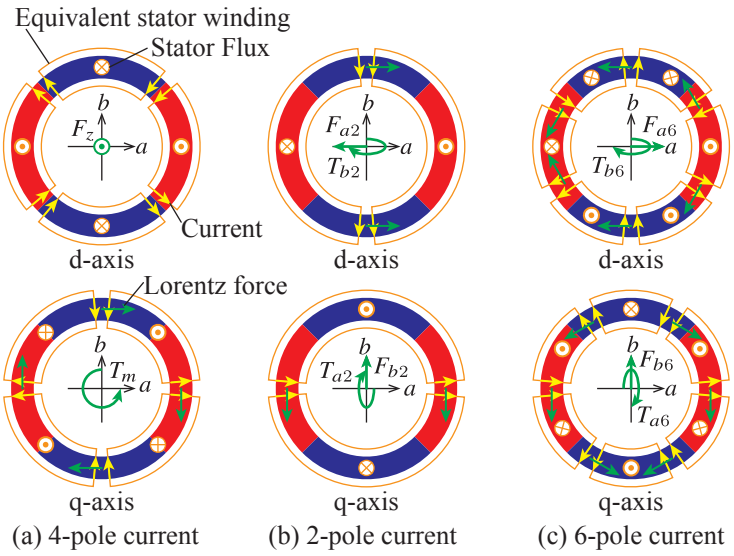

Figure 2: Principle.

In this paper, moments and forces generated by an AFSBM are analyzed theoretically by using a current sheet model. The stator currents are then calculated to control the motor torque and rotor position. Levitation and rotation tests of a prototype motor confirm the proposed method.

2 Axial-Flux Self-Bearing Motor

Fig. 1 shows the structure of the proposed AFSBM. A rotor is a flat disk, and PMs are attached to the upper side of the rotor. P denotes the number of pole pairs. A stator consists of an iron core and windings which generate rotating magnetic fields with $P-1$, P, and $P+1$ pole pairs. Sensors measure the displacements and rotation angles of the rotor, then the rotor position and posture are stabilized by feedback control.

Fig. 2 shows the principle of the generation of motor torque, axial force, radial force, and tilting moment. It illustrates a four-pole rotor as an example. The d-axis component of the four-pole current generates the magnetic field at the same as the magnetic field generated by

the rotor PM. Then it controls the axial force by changing the amplitude of the magnetic flux density in the air gap. The q-axis component of the four-pole current generates the motor torque by the Lorentz force. Two- and six-pole currents generate both radial forces and tilting moments by magnetic force and Lorentz force. However, the direction of one of them is different, e.g., F_{a2} and F_{a6} is the opposite, while T_{a2} and T_{a6} are the same. Therefore, we can control the radial forces and tilting moments by combining two- and six-pole currents.

3 Analysis of Bearing Force and Motor Torque

3.1 Coordinate System

Motor torque, axial force, radial forces, and tilting moments are theoretically analyzed.

A coordinate system is defined as Figure 3. x-y is the horizontal plane, and θ_x and θ_y are rotation around them. z is vertical, and θ is rotation around z. Since the upper surface of the rotor is the acting point of magnetic force, that point is the origin of z.

ψ is the rotation angle of the rotor. The origin of θ is at ψ. a-b is the horizontal plane fixed on the rotor, and θ_a and θ_b are rotation around them.

d-axis is the same as a-axis, and q-axis depends on the pole-pair number of the magnetic field and is at $\theta = \pi/(2P)$.

We replace the stator windings and the rotor PMs with current sheets for simplification. The positive direction of the current is from outside to inside. The direction of the magnetic flux density is the same as z, then the direction of Lorentz force becomes counterclockwise. g_0 is the air gap between the stator and rotor cores. r_o, r_i, and r are outer, inner, and average radii, respectively. The surface area of the core is represented by $A = \pi(r_o^2 - r_i^2)$.

3.2 Current and Magnetic Flux Density

For simplicity, we assume current distribution to be sinusoidal as

$$i(\theta) = I \sin(P\theta + \phi) \tag{1}$$

where I and ϕ denote the amplitude and phase of current, respectively.

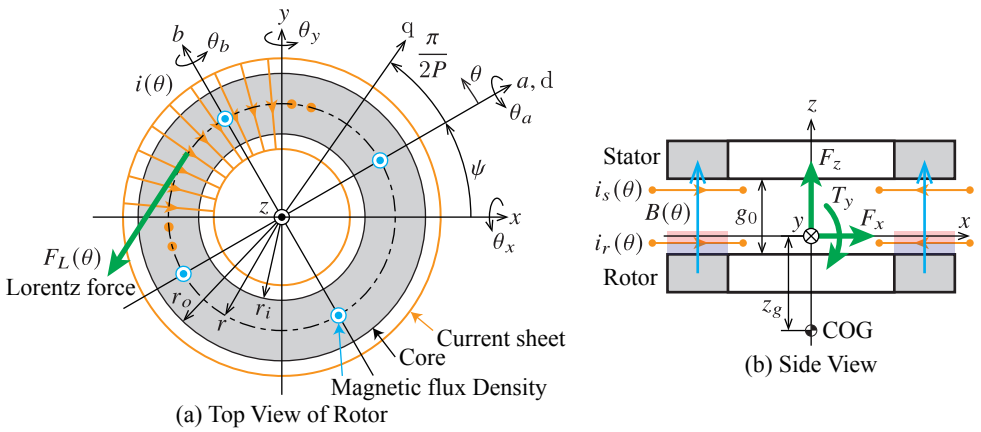

Figure 3: Coordinate system.

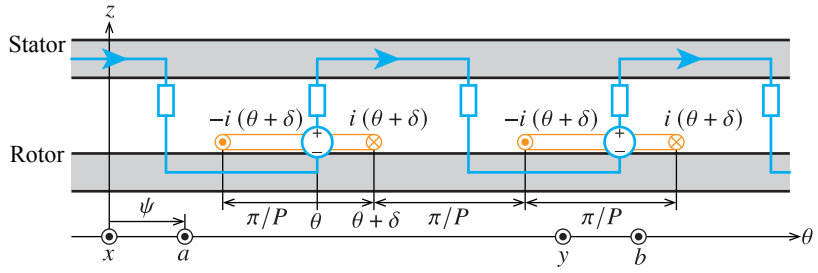

Figure 4: Magnetic circuit.

Figure 4 shows a magnetic circuit that considers only the current at $\theta+\delta+n\pi/P$, where $n = 0, 1, \cdots, P-1$. The currents at $\theta+\delta+2n\pi/P$ are $i(\theta+\delta)$, and the currents at $\theta+\delta+(2n+1)\pi/P$ are $-i(\theta+\delta)$. A blue line indicates a magnetic path generated by the currents. The cross section of the magnetic path is $A/(2P)$, and the number of air gaps in the magnetic path is $2P$, then the total magnetic resistance in the magnetic path becomes $4g_0P^2/(\mu_0 A)$. Since the number of current loops is P, the total magnetomotive force becomes $Pi(\theta+\delta)$. Consequently, the magnetic flux density at θ is calculated as

$$\Delta B(\theta) = \frac{\mu_0 A}{4g_0P^2}\ Pi(\theta+\delta)\ \frac{2P}{A} = \frac{\mu_0}{2g_0} I \sin\{P(\theta+\delta)+\phi\} \tag{2}$$

We can calculate the magnetic flux density by the whole current by integrating $\Delta B(\theta)$ with respect to δ from 0 to π/P, then we have

$$B(\theta) = \int_0^{\pi/P} \Delta B(\theta) d\delta = \frac{\mu_0}{g_0}\frac{I}{P}\cos(P\theta+\phi) \tag{3}$$

The equivalent rotor current and magnetic flux density by the rotor PM are denoted by adding subscript r. ϕ of $i_r(\theta)$ is 0 because $\cos(P\theta+\phi)$ of $B_r(\theta)$ becomes 1 at d-axis ($\theta = 0$). Hence,

$$i_r(\theta) = I_r \sin(P\theta) \tag{4}$$

The stator current, denoted by $i_s(\theta)$, is assumed to be the sum of the currents with $P-1$, P, and $P+1$ pole pairs. Each current is decomposed into d- and q-axis components. The amplitude of each component is denoted by adding subscript d, q, $P-1$, P, and $P+1$. ϕ of the d-axis component is 0, on the other hand, ϕ of the q-axis component is $-\pi/2$ because q-axis is located at $\theta = \pi/(2P)$. Then, the stator current is expressed by

$$i_s(\theta) = i_{P-1}(\theta) + i_P(\theta) + i_{P+1}(\theta) \tag{5}$$

where

$$i_{P-1}(\theta) = I_{\mathrm{d}P-1}\sin\{(P-1)\theta\} - I_{\mathrm{q}P-1}\cos\{(P-1)\theta\} \tag{6}$$
$$i_P(\theta) = I_{\mathrm{d}P}\sin(P\theta) - I_{\mathrm{q}P}\cos(P\theta) \tag{7}$$
$$i_{P+1}(\theta) = I_{\mathrm{d}P+1}\sin\{(P+1)\theta\} - I_{\mathrm{q}P+1}\cos\{(P+1)\theta\} \tag{8}$$

3.3 Force and Torque

The attractive force between the stator and the rotor of a small angle is expressed by

$$\Delta F_M = \frac{A}{4\pi\mu_0}\left\{B_r(\theta) + B_s(\theta)\right\}^2 d\theta \tag{9}$$

The axial force is calculated as

$$F_z = \int_0^{2\pi} \Delta F_M = \frac{\mu_0 A}{4g_0^2 P^2}\left\{(I_r + I_{\mathrm{d}P})^2 + I_{\mathrm{q}P}^2 + I_{\mathrm{d}P-1}^2 + I_{\mathrm{q}P-1}^2 + I_{\mathrm{d}P+1}^2 + I_{\mathrm{q}P+1}^2\right\} \tag{10}$$

The tilting moments around a and b are calculated as

$$T_a = \int_0^{2\pi} r\sin\theta\Delta F_M = \frac{\mu_0 A r}{4g_0^2 P^2}\left\{\left(-I_{\mathrm{q}P-1} + I_{\mathrm{q}P+1}\right)(I_r + I_{\mathrm{d}P}) + \left(I_{\mathrm{d}P-1} - I_{\mathrm{d}P+1}\right) I_{\mathrm{q}P}\right\} \tag{11}$$

$$T_b = \int_0^{2\pi} -r\cos\theta\Delta F_M = \frac{\mu_0 A r}{4g_0^2 P^2}\left\{\left(-I_{\mathrm{d}P-1} - I_{\mathrm{d}P+1}\right)(I_r + I_{\mathrm{d}P}) + \left(-I_{\mathrm{q}P-1} - I_{\mathrm{q}P+1}\right) I_{\mathrm{q}P}\right\} \tag{12}$$

Assume that I_r is larger than the other currents, we can neglect the product of the stator currents. Therefore,

$$F_z \approx \frac{\mu_0 A}{4g_0^2 P^2} I_r^2 + \frac{\mu_0 A}{2g_0^2 P^2} I_r I_{\mathrm{d}P} = F_{z0} + K_z I_{\mathrm{d}P} \tag{13}$$

$$T_a \approx \frac{\mu_0 A r}{4g_0^2 P^2} I_r\left(-I_{\mathrm{q}P-1} + I_{\mathrm{q}P+1}\right) = -K_t I_{\mathrm{q}P-1} + K_t I_{\mathrm{q}P+1} \tag{14}$$

$$T_b \approx \frac{\mu_0 A r}{4g_0^2 P^2} I_r\left(-I_{\mathrm{d}P-1} - I_{\mathrm{d}P+1}\right) = -K_t I_{\mathrm{d}P-1} - K_t I_{\mathrm{d}P+1} \tag{15}$$

where F_{z0} is the attractive force with zero current, and K_z and K_t are the coefficients of the force and torque, respectively.

The Lorentz force at θ is expressed by

$$F_L = (r_o - r_i)\left\{B_s(\theta) i_r(\theta) - B_r(\theta) i_s(\theta)\right\} \tag{16}$$

The motor torque is calculated as

$$T_m = \int_0^{2\pi} r F_L d\theta = \frac{\mu_0 A}{g_0 P} I_r I_{\mathrm{q}P} = K_m I_{\mathrm{q}P} \tag{17}$$

where K_m is the coefficient of the motor torque. The radial forces are calculated as

$$\begin{aligned} F_a &= \int_0^{2\pi} -F_L\sin\theta d\theta = \frac{\mu_0 A}{4g_0 P^2 r} I_r\left\{-\left(2P-1\right) I_{\mathrm{d}P-1} + \left(2P+1\right) I_{\mathrm{d}P+1}\right\} \\ &= -K_{rP-1} I_{\mathrm{d}P-1} + K_{rP+1} I_{\mathrm{d}P+1} \end{aligned} \tag{18}$$

$$\begin{aligned} F_b &= \int_0^{2\pi} F_L\cos\theta d\theta = \frac{\mu_0 A}{4g_0 P^2 r} I_r\left\{\left(2P-1\right) I_{\mathrm{q}P-1} + \left(2P+1\right) I_{\mathrm{q}P+1}\right\} \\ &= K_{rP-1} I_{\mathrm{q}P-1} + K_{rP+1} I_{\mathrm{q}P+1} \end{aligned} \tag{19}$$

where K_{rP-1} and K_{rP+1} are the coefficients of the radial forces.

A rotational transformation calculates the radial forces toward x and y and tilting moments around x and y. By rearranging the transformed equations, we have

$$\begin{bmatrix} T_y \\ F_x \end{bmatrix} = \begin{bmatrix} -K_t & -K_t \\ -K_{rP-1} & K_{rP+1} \end{bmatrix} \begin{bmatrix} I_{T_y F_x P-1} \\ I_{T_y F_x P+1} \end{bmatrix} \tag{20}$$

$$\begin{bmatrix} T_x \\ F_y \end{bmatrix} = \begin{bmatrix} -K_t & K_t \\ K_{rP-1} & K_{rP+1} \end{bmatrix} \begin{bmatrix} I_{T_x F_y P-1} \\ I_{T_x F_y P+1} \end{bmatrix} \tag{21}$$

where

$$\begin{bmatrix} I_{T_y F_x P-1} \\ I_{T_x F_y P-1} \end{bmatrix} = \begin{bmatrix} \cos\psi & \sin\psi \\ -\sin\psi & \cos\psi \end{bmatrix} \begin{bmatrix} I_{\mathrm{d}P-1} \\ I_{\mathrm{q}P-1} \end{bmatrix} \tag{22}$$

$$\begin{bmatrix} I_{T_y F_x P+1} \\ I_{T_x F_y P+1} \end{bmatrix} = \begin{bmatrix} \cos\psi & -\sin\psi \\ \sin\psi & \cos\psi \end{bmatrix} \begin{bmatrix} I_{\mathrm{d}P+1} \\ I_{\mathrm{q}P+1} \end{bmatrix} \tag{23}$$

From Eqs. (6), (8), (22) and (23), $i_{P-1}(\theta)$ and $i_{P+1}(\theta)$ are rewritten as

$$i_{P-1}(\theta) = -I_{T_y F_x P-1} \sin\{\psi - (P-1)\,\theta\} - I_{T_x F_y P-1} \cos\{\psi - (P-1)\,\theta\} \tag{24}$$

$$i_{P+1}(\theta) = I_{T_y F_x P+1} \sin\{\psi + (P+1)\,\theta\} - I_{T_x F_y P+1} \cos\{\psi + (P+1)\,\theta\} \tag{25}$$

3.4 Control of Torque and Force

Eqs. (17) and (13) show that $I_{\mathrm{q}P}$ can control T_m and $I_{\mathrm{d}P}$ can control F_z. These are the same as one-DOF active-controlled AFSBMs.

Eqs. (20) and (21) show that $I_{TxFyP-1}$ and $I_{TxFyP+1}$ generate both T_x and F_y, while $I_{TxFyP-1}$ and $I_{TxFyP+1}$ generate both T_x and F_x. Moreover, F_x and F_y generate not only the radial force but also the tilting moment around the COG of the rotor; F_y generates $-z_g F_y$ around x-axis, and F_x generates $z_g F_x$ around y-axis. Therefore, the following relationships are obtained.

$$\begin{bmatrix} T_{Gy} \\ F_{Gx} \end{bmatrix} = \begin{bmatrix} -(K_t + z_g K_{rP-1}) & -(K_t - z_g K_{rP+1}) \\ -K_{rP-1} & K_{rP+1} \end{bmatrix} \begin{bmatrix} I_{T_y F_x P-1} \\ I_{T_y F_x P+1} \end{bmatrix} \tag{26}$$

$$\begin{bmatrix} T_{Gx} \\ F_{Gy} \end{bmatrix} = \begin{bmatrix} -(K_t + z_g K_{rP-1}) & K_t - z_g K_{rP+1} \\ K_{rP-1} & K_{rP+1} \end{bmatrix} \begin{bmatrix} I_{T_x F_y P-1} \\ I_{T_x F_y P+1} \end{bmatrix} \tag{27}$$

Since both determinants of the coefficient matrices are non-zero, the solutions of the above equations are

$$\begin{bmatrix} I_{T_y F_x P-1} \\ I_{T_y F_x P+1} \end{bmatrix} = \frac{1}{-K_t\,(K_{rP-1} + K_{rP+1})} \begin{bmatrix} K_{rP+1} & K_t - z_g K_{rP+1} \\ K_{rP-1} & -(K_t + z_g K_{rP-1}) \end{bmatrix} \begin{bmatrix} T_{Gy} \\ F_{Gx} \end{bmatrix} \tag{28}$$

$$\begin{bmatrix} I_{F_y T_x P-1} \\ I_{F_y T_x P+1} \end{bmatrix} = \frac{1}{-K_t\,(K_{rP-1} + K_{rP+1})} \begin{bmatrix} K_{rP+1} & -(K_t - z_g K_{rP+1}) \\ -K_{rP-1} & -(K_t + z_g K_{rP-1}) \end{bmatrix} \begin{bmatrix} T_{Gx} \\ F_{Gy} \end{bmatrix} \tag{29}$$

These equation give the amplitudes of Eqs. (24) and (25).

4 Experimental Verification

We made and tested a prototype motor to verify the proposed control method.

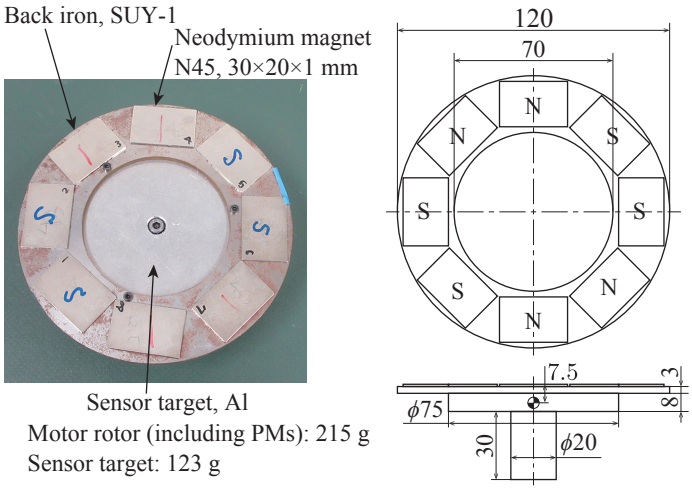

Figure 5: Rotor.

Figure 6: Stator.

4.1 Experimental Device and Control System

Fig. 5 shows the rotor. Rectangular PMs are adopted because it is easily accessible. Eight PMs are attached to a back iron to generate a four-pole magnetic field, then the pole pair number of the rotor is $P = 2$. We attached a sensor target for radial sensors under the disk.

Fig. 6 shows the stator. Twelve air core coils were made, and attached to a back iron. The location of coils are expressed as

$$\theta_k = \frac{2\pi}{12}(k-1) - \psi, \qquad k = 1, \cdots, 12 \tag{30}$$

Since the stator is the concentrated windings, the phase of the stator currents needs the phase

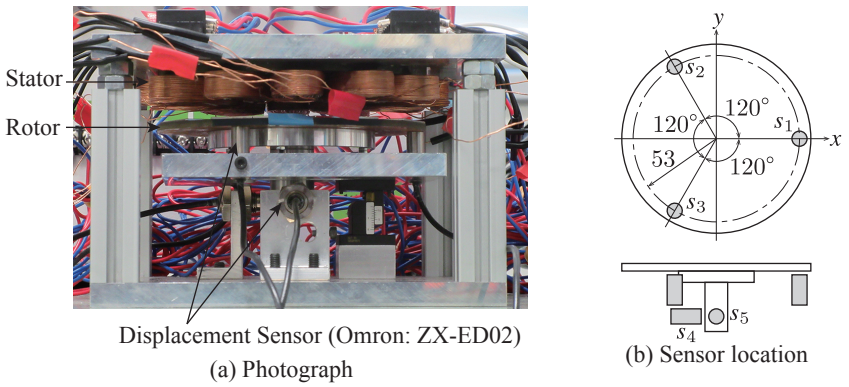

(a) Photograph (b) Sensor location

Figure 7: Whole device.

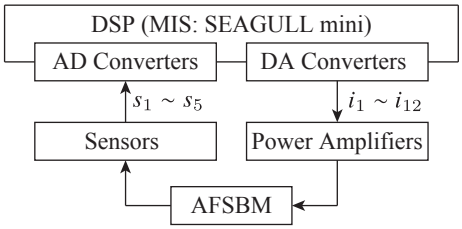

Figure 8: Control system.

lead of $\pi/2$. Therefore, each coil current can be calculated from Eqs. (7), (24), and (25) as

$$\begin{aligned} i_k = &- I_{T_y F_x 1} \cos\left\{2\psi - \frac{2\pi}{12}(k-1)\right\} + I_{T_x F_y 1} \sin\left\{2\psi - \frac{2\pi}{12}(k-1)\right\} \\ &+ I_{\mathrm{d}2} \cos\left\{2\psi - \frac{4\pi}{12}(k-1)\right\} - I_{\mathrm{q}2} \sin\left\{2\psi - \frac{4\pi}{12}(k-1)\right\} \\ &+ I_{T_y F_x 3} \cos\left\{2\psi - \frac{6\pi}{12}(k-1)\right\} - I_{T_x F_y 3} \sin\left\{2\psi - \frac{6\pi}{12}(k-1)\right\} \end{aligned} \tag{31}$$

Fig. 7 shows the whole device. Five eddy current sensors are installed under the rotor and measure the displacement of the rotor. The displacements and tilt angles about the COG of the rotor are calculated from the sensor values.

Fig. 8 shows the control system. A digital signal processor (DSP) controls the prototype motor. The DSP reads the sensor signals via analog to digital (AD) converters and calculates the current commands, then outputs the current commands to power amplifiers via digital to analog (DA) converters. The amplifiers that consist of a power operational amplifier (TI: OPA549S) with a current feedback circuit send the commanded currents through the coils. The sampling interval is 0.15 ms.

Fig. 9 shows the block diagram of the controller. The following proportional-derivative (PD) controller is adopted for position control.

$$G_{PD}(s) = K_P + K_D \frac{s}{s/\omega_b + 1} \tag{32}$$

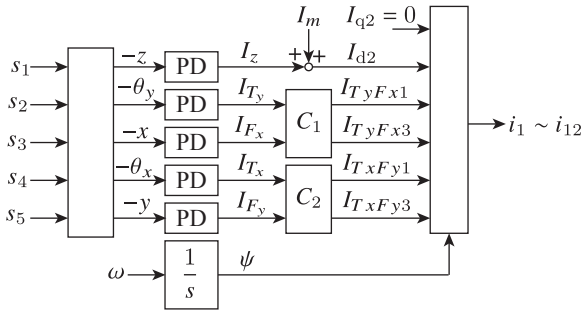

Figure 9: Controller.

	K_P	K_D	ω_b
z	2 A/mm	0.02 As/m	$2\pi \times 200$ rad/s
θ_x, θ_y	50 A/rad	0.5 As/rad	$2\pi \times 200$ rad/s
x, y	2 A/mm	0.05 As/m	$2\pi \times 200$ rad/s

Table 1: Gains of PD controllers.

where K_P is a proportional gain, K_D is a derivative gain, and ω_b is the brake frequency of the approximate differentiator. The PD controllers are converted to discrete-time transfer functions by the Tustin method and implemented to the DSP. To determine the gains experimentally, the outputs of the controllers are the control currents instead of the commands of the forces and tilting moments. Table 1 shows the gains of the controllers. C_1 and C_2 in Fig. 9 are transformation matrices, and described as

$$\begin{bmatrix} I_{T_y F_x 1} \\ I_{T_y F_x 3} \end{bmatrix} = C_1 \begin{bmatrix} I_{T_y} \\ I_{F_x} \end{bmatrix} = \begin{bmatrix} -c_T & -c_F \\ -1 & 1 \end{bmatrix} \begin{bmatrix} I_{T_y} \\ I_{F_x} \end{bmatrix} \tag{33}$$

$$\begin{bmatrix} I_{T_x F_y 1} \\ I_{T_x F_y 3} \end{bmatrix} = C_2 \begin{bmatrix} I_{T_x} \\ I_{F_y} \end{bmatrix} = \begin{bmatrix} -c_T & c_F \\ 1 & 1 \end{bmatrix} \begin{bmatrix} I_{T_x} \\ I_{F_y} \end{bmatrix} \tag{34}$$

where c_T and c_F were experimentally determined as $c_T = 1.7$ and $c_F = 0.9$. The rotation speed is controlled by the angular frequency of the stator currents.

4.2 Results of Levitation and Rotation Tests

We achieved non-contact levitation and rotation.

Fig. 10 shows step responses without rotation. These were measured by injecting step disturbance signals into the output of the PD controllers. The amplitude was 0.5 A and −0.5 A. The displacements and tilt angles settled without overshoot. These indicate that all axes are well actively controlled. There are interference between θ_x and y in case of $I_{T_x} = -0.5$ A, and θ_y and x in case of $I_{T_y} = 0.5$ A. We will investigate this problem in the future.

Fig. 11 shows the waveforms while rotation. The vibration in x and y directions increased by increasing the rotation speed. Since the radial vibration is caused by the unbalance of the rotor, the vibration became large at a high rotation speed. On the other hand, the vibration in θ_x and θ_y decreased by increasing the rotation speed due to a gyroscopic effect.

We stepped the rotation test at 900 rpm because the radial vibration became large. The rotation speed will increase by adjusting the rotor balance.

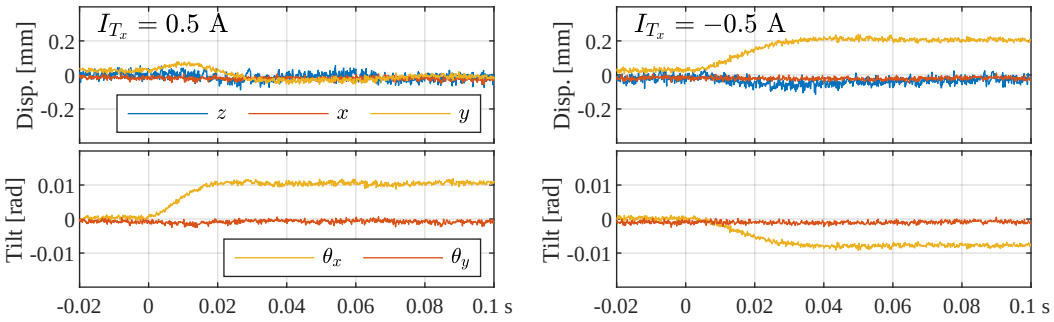

(a) I_{T_x}

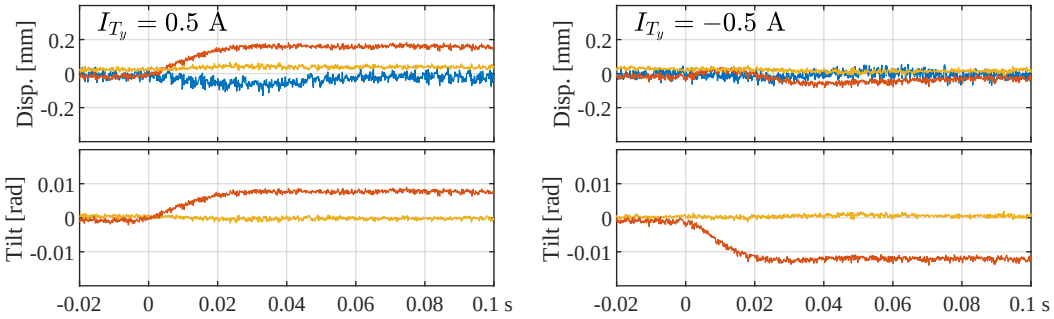

(b) I_{T_y}

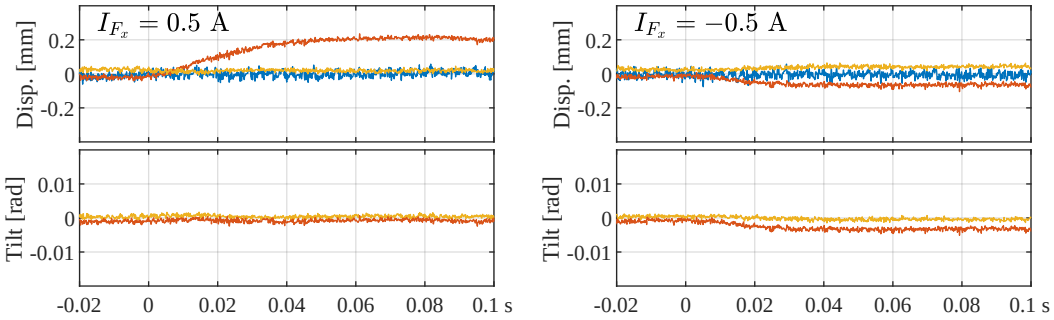

(c) I_{F_x}

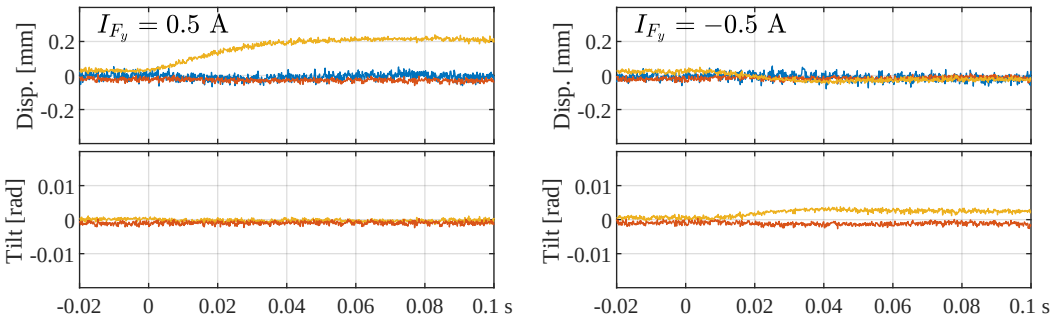

(d) I_{F_y}

Figure 10: Step responses.

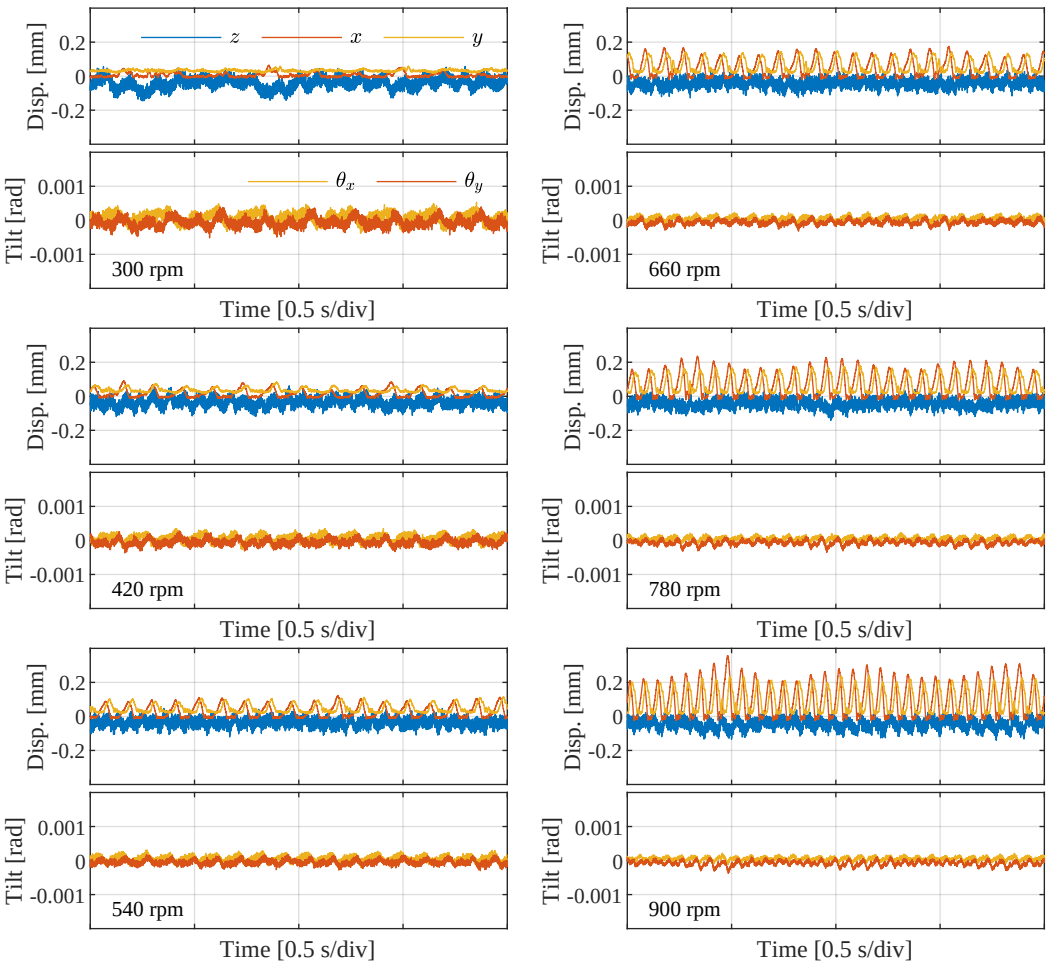

Figure 11: Waveforms while rotation.

5 Conclusions

In this paper, we introduced a five-DOF active-controlled AFSBM with a single stator. The theoretical analysis showed that the combination of the plus and minus two-pole magnetic fields controls the radial forces and tilting moments of the rotor. We succeeded in stable levitation and rotation until 900 rpm and confirmed that the proposed method is effective.

References

[1] Masahiro Osa, Toru Masuzawa, Takuya Saito, and Eisuke Tatsumi. Magnetic levitation performance of miniaturized magnetically levitated motor with 5-dof active control. *Mechanical Engineering Journal*, 2(4), 2017.

[2] Masayuki Sumino and Satoshi Ueno. Tilt control with axial self-bearing motor. *Transactions of the JSME (in Japanese)*, 2014.

[3] Satoshi Ueno, Ryo Iseki, and Changan Jiang. Stability of a tilt-controlling axial gap self-bearing motor with single-stator. *Mechanical Engineering Journal*, 4(4), 2017.

[4] Satoshi Ueno, Junichi Mameda, and Changan Jiang. Analysis and control of radial force and tilt moment for an axial-gap self-bearing motor. In *Proc. of IEEE International Electric Machines & Drives Conference, Miami, Florida, USA*, 2017.

[5] Satoshi Ueno and Yohji Okada. Characteristics of axial force and rotating torque and their control of pm type axial gap self-bearing motor. *Electrical Engineering in Japan*, 132(1):81–91, 2000.